# ON THE 2D-VALIDATION STUDY OF THE ATMOSPHERIC BOUNDARY LAYER FLOW MODEL INCLUDING POLLUTION DISPERSION

Ivo Sládek*, Karel Kozel**, Zbyněk Jaňour*

*The paper deals with a flow validation study performed using our in-house 3D-computer-code which implements mathematical and numerical model capable to simulate the atmospheric boundary layer flow in general. The validation study is related to a neutrally stratified boundary layer 2D-flow over an isolated hill with a rough wall including pollution dispersion according to Castro [1].*

*Our mathematical model is based on the system of RANS equations closed by two-equation high-Reynolds number k-ε turbulence model together with wall functions. The finite volume method and the explicit Runge-Kutta time integration method are utilized for the numerics.*

Keywords: *boundary layer flow, pollution dispersion*

## 1. Introduction

The Atmospheric Boundary Layer (ABL) can be defined as the lowest part of the Earth's atmosphere. Its thickness depends on various conditions and ranges from several hundreds of meters to approximately two kilometers. The ABL is significantly influenced by the surface, over which the wind flows, its orography and roughness, by the free stream wind and also by the vertical temperature gradient which is associated with the atmospheric thermal stratification [2], [3].

A prediction of wind field over complex terrain plays an important role in many engineering applications such as evaluation of environmental impact by pollutant dispersion, the street-canyon flows, the urban area flows etc. Because of difficulties and a high cost of experiments associated with the ABL investigation, a reliable mathematical model together with a suitable numerical method are developed and code-implemented [4], [5], [6].

The paper is mainly devoted to validation of the mathematical/numerical model for the ABL flow in general. It is quite difficult to perform such a validation using some reliable field experimental data. Hence, simplified 2D-test-case with reference experimental/numerical data has been chosen, see the section 6. Some results have already been published in [7].

The reference numerical data due to [1] are based on:

– 2D-validation of velocity-field: two-equation high-Re standard k-ε turbulence modelling with wall-functions

* Ing. I. Sládek, Ph.D., prof. RNDr. Z. Jaňour, DrSc., Institute of Thermodynamics, Academy of Sciences, Dolejškova 1402/5, ZIP 18200, Prague 8

** prof. RNDr. K. Kozel, DrSc., Department of Technical Mathematics (12101), Faculty of Mechanical Engineering, Czech Technical University, Karlovo náam. 13/B-219, ZIP 12135, Prague 2

– 3D-validation of concentration field : based on the above 2D-velocity field simply redistributed in the 'third' span-wise direction to respect a point nature of the pollutant source.

## 2. Mathematical formulation in 3D

The flow itself is assumed to be turbulent, viscous, incompressible, stationary and neutrally stratified as well. The mathematical model is based on RANS approach and the governing equations can be formulated in the conservative, dimensional and vector form

$$(\vec{F})_{\mathrm{x}} + (\vec{G})_{\mathrm{y}} + (\vec{H})_{\mathrm{z}} = (\vec{R})_{\mathrm{x}} + (\vec{S})_{\mathrm{y}} + (\vec{T})_{\mathrm{z}} \ , \tag{1}$$

where the terms $\vec{F}$, $\vec{G}$, $\vec{H}$ represent the physical inviscid fluxes and $\vec{R}$, $\vec{S}$, $\vec{T}$ denote the viscous fluxes. When expanding all the above vector terms in (1), we get

$$\begin{pmatrix} u \\ u^2 + \frac{p}{\varrho} \\ u\,v \\ u\,w \\ u\,C \end{pmatrix}_{\mathrm{x}} + \begin{pmatrix} v \\ v\,u \\ v^2 + \frac{p}{\varrho} \\ v\,w \\ v\,C \end{pmatrix}_{\mathrm{y}} + \begin{pmatrix} w \\ w\,u \\ w\,v \\ w^2 + \frac{p}{\varrho} \\ w\,C \end{pmatrix}_{\mathrm{z}} = \begin{pmatrix} 0 \\ K\,u_{\mathrm{x}} \\ K\,v_{\mathrm{x}} \\ K\,w_{\mathrm{x}} \\ \tilde{K}\,C_{\mathrm{x}} \end{pmatrix}_{\mathrm{x}} + \begin{pmatrix} 0 \\ K\,u_{\mathrm{y}} \\ K\,v_{\mathrm{y}} \\ K\,w_{\mathrm{y}} \\ \tilde{K}\,C_{\mathrm{y}} \end{pmatrix}_{\mathrm{y}} + \begin{pmatrix} 0 \\ K\,u_{\mathrm{z}} \\ K\,v_{\mathrm{z}} \\ K\,w_{\mathrm{z}} \\ \tilde{K}\,C_{\mathrm{z}} \end{pmatrix}_{\mathrm{z}} \ . \tag{2}$$

The system (2) is then modified in order to be solved by the artificial compressibility method

$$\begin{pmatrix} \frac{p}{\beta^2} \\ u \\ v \\ w \\ C \end{pmatrix}_{\mathrm{t}} + \begin{pmatrix} u \\ u^2 + \frac{p}{\varrho} \\ u\,v \\ u\,w \\ u\,C \end{pmatrix}_{\mathrm{x}} + \begin{pmatrix} v \\ v\,u \\ v^2 + \frac{p}{\varrho} \\ v\,w \\ v\,C \end{pmatrix}_{\mathrm{y}} + \begin{pmatrix} w \\ w\,u \\ w\,v \\ w^2 + \frac{p}{\varrho} \\ w\,C \end{pmatrix}_{\mathrm{z}} = \begin{pmatrix} 0 \\ K\,u_{\mathrm{x}} \\ K\,v_{\mathrm{x}} \\ K\,w_{\mathrm{x}} \\ \tilde{K}\,C_{\mathrm{x}} \end{pmatrix}_{\mathrm{x}} + \begin{pmatrix} 0 \\ K\,u_{\mathrm{y}} \\ K\,v_{\mathrm{y}} \\ K\,w_{\mathrm{y}} \\ \tilde{K}\,C_{\mathrm{y}} \end{pmatrix}_{\mathrm{y}} + \begin{pmatrix} 0 \\ K\,u_{\mathrm{z}} \\ K\,v_{\mathrm{z}} \\ K\,w_{\mathrm{z}} \\ \tilde{K}\,C_{\mathrm{z}} \end{pmatrix}_{\mathrm{z}} \ , \tag{3}$$

where $\vec{W} = (p/\beta^2, u, v, w, C\,)^{\mathrm{T}}$ stands for the vector of unknown variables, namely the pressure $p$, the velocity vector $\vec{V} = (u, v, w\,)^{\mathrm{T}}$ and the passive pollutant concentration $C$ (measured in [kg/m$^3$]), the density reads $\varrho = \mathrm{const}$. The parameters $K$, $\tilde{K}$ refer to the turbulent diffusion coefficients, see equation (17), and the parameter $\beta$ is related to the artificial sound speed.

The system (3) is solved in the computational domain $\Omega$ under a stationary boundary conditions for $t \to \infty$ ($t$ is an artificial time variable) to obtain the expected steady-state solution for all the unknown variables involved in the vector $\vec{W}$.

## 3. Numerical treatment

A structured non-orthogonal grids made of hexahedral control cells are used for all computations. The finite volume method of cell-centered type together with a multi-stage explicit Runge-Kutta time integration scheme have been applied to solve system (3), as reported in [4], [14]. Integration of (3) over each control cell $\Omega_{ijk}$ then gives

$$\int\limits_{\Omega_{ijk}} \vec{W}_t \,\mathrm{d}V = -\int\limits_{\Omega_{ijk}} \left[ (\vec{F} - K\,\vec{R})_{\mathrm{x}} + (\vec{G} - K\,\vec{S})_{\mathrm{y}} + (\vec{H} - \vec{T})_{\mathrm{z}} \right] \mathrm{d}V \ . \tag{4}$$

This identity can be rewritten using the divergence theorem and the mean value theorem

$$\vec{W}_{\mathrm{t}}\Big|_{ijk} = -\frac{1}{\mu_{ijk}} \oint\limits_{\partial\Omega_{ijk}} \left[(\vec{F} - K\,\vec{R})\,\mathrm{d}S_1 + (\vec{G} - K\,\vec{S})\,\mathrm{d}S_2 + (\vec{H} - K\,\vec{T})\,\mathrm{d}S_3\right] , \tag{5}$$

where $\vec{W}_{\mathrm{t}}|_{ijk}$ is the mean value of $\vec{W}_{\mathrm{t}}$ over the cell $\Omega_{ijk}$ and $\mu_{ijk} = \int_{\Omega_{ijk}} \mathrm{d}V$ denotes the volume of control cell. After space discretization of (5), we come up with a set of semi-discrete system of ordinary differential equations for each $\Omega_{ijk}$

$$\vec{W}_{\mathrm{t}}\Big|_{ijk}(t) = \mathbf{L}\vec{W}_{ijk}(t) , \tag{6}$$

where $\mathbf{L}\vec{W}_{ijk}$ denotes the operator approximating the right-hand side of (5), which has the following form

$$\mathbf{L}\vec{W}_{ijk} = -\frac{1}{\mu_{ijk}} \sum_{l=1}^{6} \Big[(\tilde{\vec{F}}_l - K_l\,\tilde{\vec{R}}_l)\,\Delta S_1^l + (\tilde{\vec{G}}_l - K_l\,\tilde{\vec{S}}_l)\,\Delta S_2^l + (\tilde{\vec{H}}_l - K_l\,\tilde{\vec{T}}_l)\,\Delta S_3^l\Big]. \tag{7}$$

All the symbols in equation (7) denoted with subscript or superscript $l$ refer to the $l$-th cell face of $\Omega_{ijk}$ and ($\Delta S_1^l$, $\Delta S_2^l$, $\Delta S_3^l$) represents the $l$-th outer normal vector.

The inviscid numerical fluxes $\tilde{\vec{F}}_l$,$\tilde{\vec{G}}_l$,$\tilde{\vec{H}}_l$ through the $l$-th face of $\Omega_{ijk}$ are computed as an average from the mean value over cell $\Omega_{ijk}$ and the mean value over the neighbor cell sharing the $l$-th face with cell $\Omega_{ijk}$, thus we get

$$\begin{aligned}
\tilde{\vec{F}}_l &= \frac{1}{2}\left(\vec{F}|_{\Omega_{ijk}} + \vec{F}|_{l-\text{th neighbor of }\Omega_{ijk}}\right) , \\
\tilde{\vec{G}}_l &= \frac{1}{2}\left(\vec{G}|_{\Omega_{ijk}} + \vec{G}|_{l-\text{th neighbor of }\Omega_{ijk}}\right) , \\
\tilde{\vec{H}}_l &= \frac{1}{2}\left(\vec{H}|_{\Omega_{ijk}} + \vec{H}|_{l-\text{th neighbor of }\Omega_{ijk}}\right) , \qquad l = 1,\ldots,6 .
\end{aligned} \tag{8}$$

On the other hand, to compute the viscous fluxes at the $l$-th face of cell $\Omega_{ijk}$, one has to know the derivatives of the velocity components at all six faces of each hexahedral control cell. The derivatives are evaluated using the dual control volumes of the octahedral shape denoted by $\bar{\Omega}_{ijk}^{(l)}$, see the Figure 1.

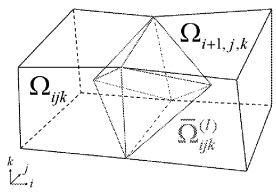


*Fig.1: Dual control volume*

An example of the $x$-derivative computation of the $u$-velocity component at the $l$-th face of the hexahedral computational cell $\Omega_{ijk}$ then reads

$$u_{\mathrm{x}}|_{ijk}^{(l)} = \int\limits_{\bar{\Omega}_{ijk}^{(l)}} u_{\mathrm{x}}(x,y,z,t)\,\mathrm{d}\bar{V} = \oint\limits_{\partial\bar{\Omega}_{ijk}^{(l)}} u\,\mathrm{d}\bar{S}_1 \approx \sum_{q=1}^{8} \tilde{u}_q^{(l)}\,\Delta\bar{S}_1^{(l,\,q)} , \tag{9}$$

where the index $q$ goes through all faces of the dual octahedral control volume $\bar{\Omega}_{ijk}^{(l)}$ and $\Delta S_1^{(l,\,q)}$ abbreviates the first component of the $q$-th outer normal vector related to the $q$-th face of the dual cell.

Finally, the 3-stage explicit Runge-Kutta time integration scheme is applied to system (6) of ODE's

$$\begin{aligned}
\vec{W}_{ijk}^{(0)} &= \vec{W}_{ijk}^{n} \ , \\
\vec{W}_{ijk}^{(1)} &= \vec{W}_{ijk}^{(0)} - \alpha_1 \, \Delta t \, \mathbf{B}\vec{W}_{ijk}^{(0)} \ , \\
\vec{W}_{ijk}^{(2)} &= \vec{W}_{ijk}^{(0)} - \alpha_2 \, \Delta t \, \mathbf{B}\vec{W}_{ijk}^{(1)} \ , \\
\vec{W}_{ijk}^{(3)} &= \vec{W}_{ijk}^{(0)} - \alpha_3 \, \Delta t \, \mathbf{B}\vec{W}_{ijk}^{(2)} \ , \\
\vec{W}_{ijk}^{n+1} &= \vec{W}_{ijk}^{(3)} \ ,
\end{aligned} \tag{10}$$

where $\alpha_1 = \alpha_2 = 1/2$, $\alpha_3 = 1$. This method is second order accurate both in time and space on an orthogonal grids. The operator $\mathbf{B}\vec{W}_{ijk}^{(m)}$ defines a steady residual in the $m$-th stage ($m$ = 1,...,3) for each control cell $\Omega_{ijk}$ and it can be written as

$$\mathbf{B}\vec{W}_{ijk}^{(m)} = \mathbf{L}\vec{W}_{ijk}^{(m)} + \mathbf{D}\vec{W}_{ijk}^{(0)} \ , \tag{11}$$

where $\mathbf{L}\vec{W}_{ijk}$ corresponds to the operator resulting from the space discretization of system (5) and the second term $\mathbf{D}\vec{W}_{ijk}$ abbreviates the artificial viscosity contribution either of 4-th order (for the pressure-velocity flow-field) or 2-nd order (for the concentration field)

$$\begin{aligned}
\mathbf{D}\vec{W}_{ijk} = &-\varepsilon_{\mathrm{x}}^{(4)} \, \Delta x^4 \, \vec{W}_{\mathrm{xxxx}}\big|_{ijk} - \varepsilon_{\mathrm{y}}^{(4)} \, \Delta y^4 \, \vec{W}_{\mathrm{yyyy}}\big|_{ijk} - \varepsilon_{\mathrm{z}}^{(4)} \, \Delta z^4 \, \vec{W}_{\mathrm{zzzz}}\big|_{ijk} + \\
&+ \varepsilon_{\mathrm{x}}^{(2)} \, \Delta x^2 \, \vec{W}_{\mathrm{xx}}\big|_{ijk} + \varepsilon_{\mathrm{y}}^{(2)} \, \Delta y^2 \, \vec{W}_{\mathrm{yy}}\big|_{ijk} + \varepsilon_{\mathrm{z}}^{(2)} \, \Delta z^2 \, \vec{W}_{\mathrm{zz}}\Big|_{ijk} \ ,
\end{aligned} \tag{12}$$

where $\varepsilon^{(4)}$, $\varepsilon^{(2)}$ denote constant coefficients to be tuned empirically and all the derivatives are substituted by central differences as it is shown hereafter for 1D case for sake of simplicity

$$\mathbf{D}\vec{W}_i = -\varepsilon_{\mathrm{x}}^{(4)} \left[\vec{W}_{i-2} - 4\,\vec{W}_{i-1} + 6\,\vec{W}_i - 4\,\vec{W}_{i+1} + \vec{W}_{i+2}\right] + \varepsilon_{\mathrm{y}}^{(2)} \left[\vec{W}_{i-1} - 2\,\vec{W}_i + \vec{W}_{i+1}\right] . \tag{13}$$

This term removes a high frequency oscillations and wiggles generated in the computed flow-field near a sharp corners in geometry or in the vicinity of a large gradients. If not smoothed, the oscillations, resulting mainly due to the central type of differencing of convective terms in (3), may completely destroy the numerical solution. Remark also, the artificial viscosity term does not change the order of the applied numerical scheme.

The stability limit criterion, valid for a regular orthogonal meshes, is applied due to the explicit numerical formulation

$$\Delta t \le \min_{\Omega_{ijk}} \frac{CFL}{\dfrac{\varrho_{\mathrm{A}}}{\Delta x} + \dfrac{\varrho_{\mathrm{B}}}{\Delta y} + \dfrac{\varrho_{\mathrm{C}}}{\Delta z} + 2\,K\left(\dfrac{1}{\Delta x^2} + \dfrac{1}{\Delta y^2} + \dfrac{1}{\Delta z^2}\right)} \ , \tag{14}$$

where $\varrho_{\mathrm{A}}$, $\varrho_{\mathrm{B}}$, $\varrho_{\mathrm{C}}$ refer to the spectral radii of the inviscid Jacobi matrices and $CFL = 2$, as reported in [14].

## 4. Turbulence model

Closure of the system (3) is performed by standard high-Reynolds $k$-$\varepsilon$ model formulated using wall-functions [3]. Hence, two additional transport equations are added to the system (3) for the turbulent kinetic energy abbreviated by $k$ and for the rate of dissipation of turbulent kinetic energy denoted by $\varepsilon$

$$\left(k\,u\right)_{\mathrm{x}} + \left(k\,v\right)_{\mathrm{y}} + \left(k\,w\right)_{\mathrm{z}} = \left(K^{(k)}\,k_{\mathrm{x}}\right)_{\mathrm{x}} + \left(K^{(k)}\,k_{\mathrm{y}}\right)_{\mathrm{y}} + \left(K^{(k)}\,k_{\mathrm{z}}\right)_{\mathrm{z}} + P - \varepsilon\ , \tag{15}$$

$$\left(\varepsilon\,u\right)_{\mathrm{x}} + \left(\varepsilon\,v\right)_{\mathrm{y}} + \left(\varepsilon\,w\right)_{\mathrm{z}} = \left(K^{(\varepsilon)}\,\varepsilon_{\mathrm{x}}\right)_{\mathrm{x}} + \left(K^{(\varepsilon)}\,\varepsilon_{\mathrm{y}}\right)_{\mathrm{y}} + \left(K^{(\varepsilon)}\,\varepsilon_{\mathrm{z}}\right)_{\mathrm{z}} + C_{\varepsilon 1}\,\frac{\varepsilon}{k}\,P - C_{\varepsilon 2}\,\frac{\varepsilon^2}{k}\ , \tag{16}$$

where $P$ denotes the turbulent production term $P = \tau_{ij}\,\partial v_i/\partial x_j$ for the Reynolds stress written as $\tau_{ij} = -2\,k\,\delta_{ij}/3 + \nu_{\mathrm{T}}\,(\partial v_i/\partial x_j + \partial v_j/\partial x_i)$ and the terms $\tilde{K}$, $K^{(k)}$, $K^{(\varepsilon)}$, $\nu_{\mathrm{T}}$ stand for the diffusion coefficients and the turbulence viscosity

$$\tilde{K} = \nu + \frac{\nu_{\mathrm{T}}}{\sigma_{\mathrm{C}}}\ , \qquad K^{(k)} = \nu + \frac{\nu_{\mathrm{T}}}{\sigma_{\mathrm{k}}}\ , \qquad K^{(\varepsilon)} = \nu + \frac{\nu_{\mathrm{T}}}{\sigma_{\varepsilon}}\ , \qquad \nu_{\mathrm{T}} = C_{\mu}\,\frac{k^2}{\varepsilon}\ , \tag{17}$$

where the parameter $\sigma_{\mathrm{C}} = 0.74$ denotes the turbulent Prandtl number. The closure coefficients for the turbulence model are described in [1]

$$C_{\mu} = 0.09\ , \qquad \sigma_{\mathrm{k}} = 1.0\ , \qquad \sigma_{\varepsilon} = 1.11\ , \qquad C_{\varepsilon 1} = 1.44\ , \qquad C_{\varepsilon 2} = 1.92\ . \tag{18}$$

## 5. Boundary conditions

The system (3)+(15)+(16) is solved with the following boundary conditions [1]

– Inlet : $u = \dfrac{u^*}{\kappa}\,\ln\left(\dfrac{z}{z_0}\right)$, $v = 0$, $w = 0$, $k = \dfrac{u^{*2}}{\sqrt{C_{\mu}}}\left(1 - \dfrac{z}{D}\right)^2$, $\varepsilon = \dfrac{C_{\mu}^{3/4}\,k^{3/2}}{\kappa\,z}$,

– Outlet : homogeneous Neumann conditions for all quantities,

– Top : $u = U_0$, $v = 0$, $\dfrac{\partial w}{\partial z} = 0$, $\dfrac{\partial k}{\partial z} = 0$, $\dfrac{\partial \varepsilon}{\partial z} = 0$, $\dfrac{\partial C}{\partial z} = 0$,

– Wall : standard wall functions are applied and $\dfrac{\partial C}{\partial n} = 0$ for the concentration,

where $U_0$ represents the free-stream velocity magnitude, $u^*$ is the friction velocity, $\kappa = 0.40$ denotes the von Kármán constant, $z_0$ represents the roughness parameter and the parameter $D$ refers to the boundary layer depth.

The wall-functions enable to apply a wall-coarser grids and near-wall profiles of computed quantities can be reconstructed via an algebraic profiles [3], [14]. Hence, the CPU time of computer simulations can be significantly reduced. Remark that true and correct use of this approach is for non-separated turbulent boundary layer flows only, where the production of turbulent kinetic energy is in balance with its dissipation. The wall-functions of different forms are widely used in engineering practice for complex flow applications [8].

## 6. Validation

• The reference experimental data due to Khurshudyan [9] and corrected by Trombetti [10] are also available in the ERCOFTAC database [15]. Moreover, Castro performed flow and

pollution dispersion reference numerical computations [1]. Some results have already been published in [7].

• The computational domain extended distance $\pm 40\,H$ up and downwind of the hill summit and to vertical height $13.7\,H$, where $H = 0.117\,\mathrm{m}$ is hill height. The hill H3 of maximum slope of 26° has been chosen. Two grids have been tested and the results compared, both of them including 400×80 cells and uniformly expanding upwind, downwind and vertically according to the following expansion ratio parameters $ax, az$ in the stream-wise and the wall-normal directions.

Grid-A : wall coarser grid, $ax = 1.01$, $az = 1.032$ leading to $\Delta x_{\min} = 7.4\,\mathrm{mm}$, $\Delta z_{\min} = 4.2\,\mathrm{mm}$ and in terms of wall-units $\Delta x^+_{\min} = 87.8$, $\Delta z^+_{\min} = 49.8$ based on $\nu$ and $u^*$,

Grid-B : wall finer grid, $ax = 1.01$, $az = 1.071$ leading to $\Delta x_{\min} = 7.4\,\mathrm{mm}$, $\Delta z_{\min} = 0.43\,\mathrm{mm}$ and in terms of wall-units $\Delta x^+_{\min} = 87.8$, $\Delta z^+_{\min} = 5.1$, here $\Delta z_{\min}$ is comparable as in the Castro's case.

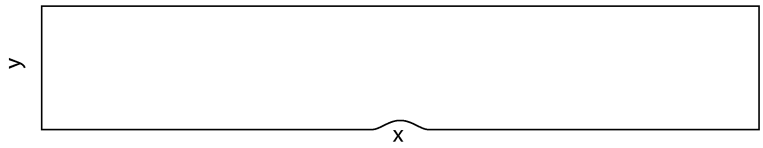


*Fig.2: Whole 2D-computational domain of length and height 9.36 m and 1.6 m, flow is assumed from left to right, hill summit is at $x = 0\,m$ and $y = 0.117\,m$*

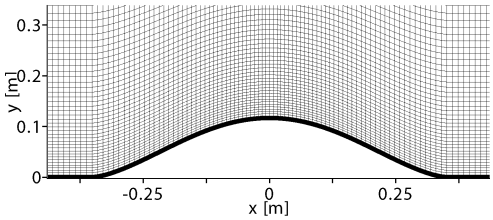


*Fig.3: Zoom to non-uniform wall-coarser Grid-A*

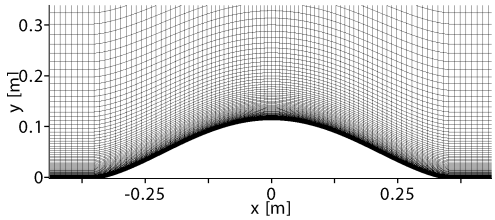


*Fig.4: Zoom to non-uniform wall-finer Grid-B*

• The flow-field input parameters are : the free-stream air velocity $U_0 = 4\,\mathrm{m/s}$, the boundary layer depth $D = 1\,\mathrm{m}$, the friction velocity $u^* = 0.178\,\mathrm{m/s}$, the roughness parameters $z_0 = 0.16\,\mathrm{mm}$ and the Reynolds number $Re = 31200$, which based on $U_0$, hill height $H = 117\,\mathrm{mm}$ and the air kinematic viscosity $\nu = 1.5{\times}10^{-5}\,\mathrm{m^2/s}$. The inlet profiles of $u$, $k$ and $\varepsilon$ have been constructed, according to relations in the section 5, to extend the boundary layer depth $D$ and then the uniform and continuous extrapolation have been performed up to the top of computational domain.

• The concentration input parameters are : totally three different heights of linear source (2D-computations) have been assumed at the downwind side of hill : $x_{\mathrm{s}} = 3\,H$ and $z_{\mathrm{s}} = 0.25\,H, 0.5\,H, 1.0\,H$. Normalization of the concentration field is performed for presentation purposes either as a) $\chi = C\,U_0\,H^2/Q$, where $Q$ denotes the source intensity ($[\mathrm{kg/m^3/s}]$) or b) by the corresponding maximum glc (ground-level-concentration) over flat terrain (additionally computed for all three source heights) as $C/C_{0,\max}$.

• Concentration source treatment : Castro performed all his concentration simulations using the 3D-grid respecting point nature of the source. Actually, Castro redistributed the

2D-flow-field uniformly in the lateral $y$-direction for that purpose. This is also our near-future target, however we first started with CPU-time less consuming 2D-concentration simulations based on frozen pressure-velocity flow-field data on a given grid. Therefore, comparison between the Castro's and ours numerical predictions can be performed at a qualitative level only and not quantitatively. The Grid-B has been used for all concentration simulations as in [1].

### 6.1. Remark on validation

Different validation study of the mathematical model (3) (without dispersion model) has been already performed in the past. Another two types of turbulence models were used based on $k$-$\varepsilon$ model in the low-Reynolds-number formulation and the algebraic turbulence model due to Baldwin and Lomax.

The validation was based on the ERCOFTAC test case due to Almeida of fully developed channel water-flow over 2D-hill mounted on bottom wall [15]. The numerical results were compared to the reference experimental data [11] and also to the reference numerical data [12]. Our numerical predictions were published eg. in [13] and [14].

## 7. Some numerical results for velocity field

A fairly large separation zone develops behind hill, see the Figures 5 and 6 for comparison between Grid-A and Grid-B predictions. Notice that measured reattachment length was $x_\mathrm{r} = 6.5\,H$ and the Castro's numerical prediction was $x_\mathrm{r} = 4.1\,H$.

The stream-wise $u$-velocity profiles at the hill summit and at half of measured recirculation bubble are shown in Figures 7, 8, 9 and 10.

The near-wall speed-up effect at the hill summit is totally smeared on the coarse Grid-A profile, see the Figure 7. However, it is well captured on the fine Grid-B profile. Both profiles on the next Figure 8 follow well the experimental data above the height of the recirculation zone. However, there is different behavior in the bubble due to different prediction of reattachment points on the two grids.

The wall-normal velocity profile comparison can be seen on the Figure 9 where much better agreement is achieved on the coarser Grid-A profile compared to the fine Grid-B profile. Both profiles follow well the experimental data on the next Figure 10.

There is generally the under-prediction of the turbulent kinetic energy $k$ at the hill summit on both grids as presented on the Figure 11. This finding is well comparable with Castro's numerical predictions [3], p. 845. On the other hand, there is an excessive production of $k$ in the wall-vicinity for our both profiles as outlined on the Figure 12.

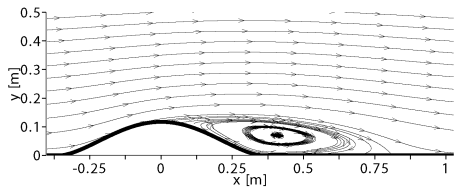


*Fig.5: Zoom of separation zone behind hill on wall-coarser Grid-A, reattachment $x_r = 6.84\,H$*

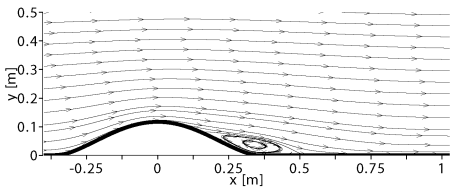


*Fig.6: Zoom of separation zone behind hill on wall-finer Grid-B, reattachment $x_r = 4.18\,H$*

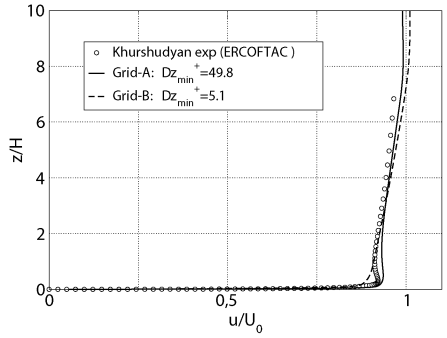


*Fig.7: Stream-wise $u/U_0$-velocity profiles at hill summit $x = 0\,H$*

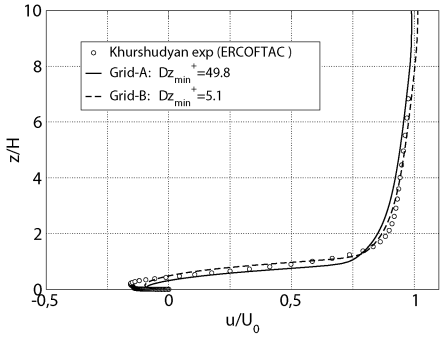


*Fig.8: Stream-wise $u/U_0$-velocity profiles at half of measured recirculation zone $x = 3\,H$*

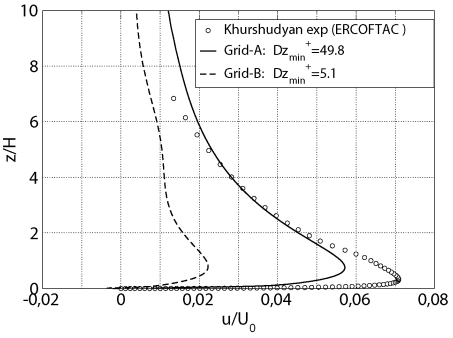


*Fig.9: Wall-normal $w/U_0$-velocity profiles at hill summit $x = 0\,H$*

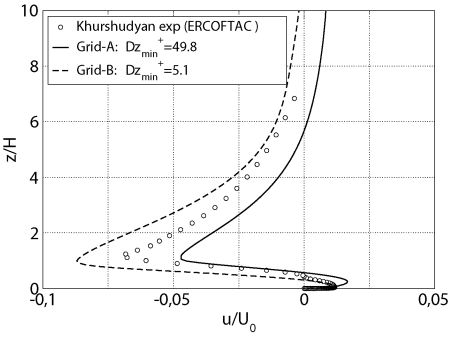


*Fig.10: Wall-normal $w/U_0$-velocity profiles at half of measured recirculation zone $x = 3\,H$*

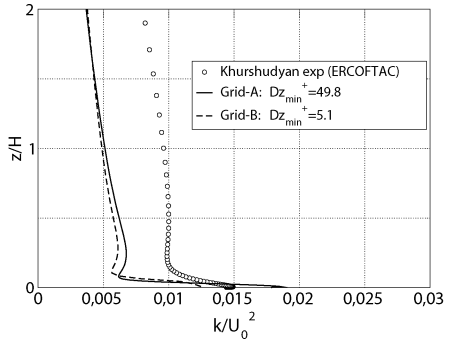


*Fig.11: Turbulent kinetic energy $k/U_0^2$-profiles at hill summit $x = 0\,H$*

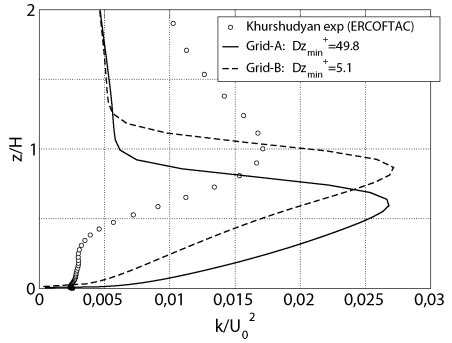


*Fig.12: Turbulent kinetic energy $k/U_0^2$-profiles at half of measured recirculation zone $x = 3\,H$*

## 8. Some numerical results for concentration field

The following figures have been created to be directly compared to similar figures published by Castro in [3], p. 847. A qualitative matching exists between our predictions and Castro's results. However, there is disagreement when trying to compare them quantitatively due to linear nature of our source (2D-computation) and point nature of the Castro's reference case (3D-computation).

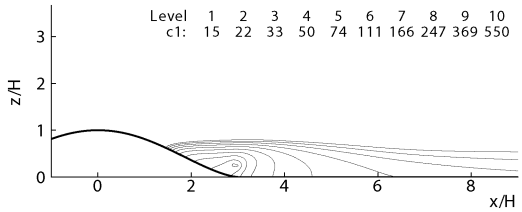


*Fig.13: Computed contours of* $\chi = C\,U_0\,H^2/Q$ *with exponential scale starting at* $\chi = 15$ *for source heights* $0.25\,H$

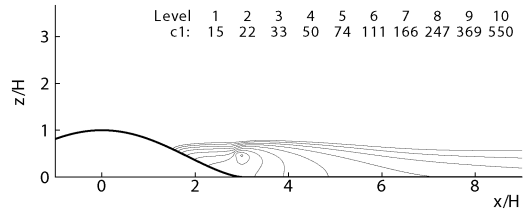


*Fig.14: Computed contours of* $\chi = C\,U_0\,H^2/Q$ *with exponential scale starting at* $\chi = 15$ *for source heights* $0.5\,H$

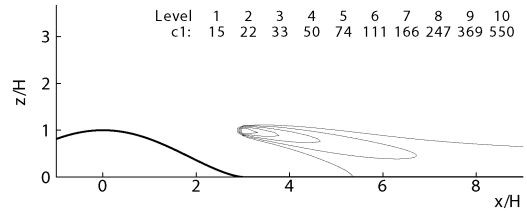


*Fig.15: Computed contours of* $\chi = C\,U_0\,H^2/Q$ *with exponential scale starting at* $\chi = 15$ *for source heights* $1.0\,H$

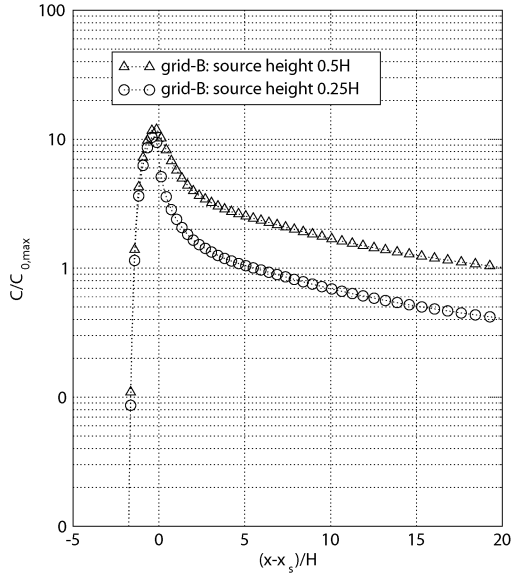


*Fig.16: Ground-level-concentrations (glc) with source at heights* $0.25\,H$ *and* $0.5\,H$*, normalized by corresponding maximum glc over flat terrain*

It is also interesting to compare our and Castro's reference ground-level-concentration (glc) profiles, the Figure 16 to be directly compared with similar figure published by Castro in [3], p. 847. Both well predict the peak position of concentration distribution which is slightly shifted upstream from the source $x$-location. The peak value is called the 'terrain amplification factor'. One can also see much slower plume decay in our case (2D-computation) compared to the Castro's reference one (3D-computation).

## 9. Conclusion

The key findings of the validation study described above are as follows. The reattachment point is very sensible to the wall grid resolution. The Castro's value is $x_\mathrm{r} = 4.1\,H$ for the standard $k$-$\varepsilon$ model and the experimental one is $x_\mathrm{r} = 6.5\,H$. We achieved $x_\mathrm{r} = 6.84\,H$ on the wall-coarser Grid-A and $x_\mathrm{r} = 4.18\,H$ on the wall-finer Grid-B. The preliminary 2D-concentration computations have shown a qualitative agreement with the target Castro's numerical predictions. Also the effect of near-ground 'terrain amplification factor' is well captured if the normalization is done by the maximum ground-level-concentrations over flat terrain. Its maximum is slightly shifted upstream of the pollutant source and this is a feature that cannot be captured by any simple Gaussian-plume model. The validation concentration 3D-simulations will proceed soon.

## Acknowledgment

The presented work was supported by the Grant No. 1ET400760405 and Research Plan 6840770010.

## Notation

| | |
|---|---|
| $\|^n$ | : superscript related to time level |
| $\|^{"}$ | : superscript related to perturbation |
| $\|^*$ | : superscript related to friction |
| $\|_{1,\,2,\,3}$ | : subscripts related to $x, y, z$-axis directions |
| $\|_{i,\,j,\,k}$ | : subscripts related to reference directions |
| $\|_{\mathrm{t,\,x,\,y,\,z}}$ | : subscripts related to derivative in time and in space |
| $\|_0$ | : subscript related to free-stream |
| $\|_l$ | : subscript related to the $l$-th face of control volume |
| $\alpha_i$ | : Runge-Kutta coefficients |
| $\beta$ | : artificial sound speed |
| $\kappa$ | : von Kármán constant |
| $\nu$, $\nu_\mathrm{T}$ | : kinematic laminar viscosity, turbulent viscosity |
| $\varrho$ | : density |
| $\sigma_\mathrm{C}$ | : turbulent Prandtl number for concentration |
| $C_\mu$, $\sigma_\mathrm{k}$, $\sigma_\varepsilon$, $C_{\varepsilon 1}$, $C_{\varepsilon 2}$ | : closure coefficients for turbulence model |
| $\varepsilon$ | : artificial diffusion coefficients, dissipation of turbulent kinetic energy |
| $k$ | : turbulent kinetic energy |
| $\Delta t$ | : time step |
| $\Delta x$, $\Delta y$, $\Delta z$ | : stream-wise, span-wise, wall-normal space increments |
| $\Omega$ | : computational domain |
| $\Omega_{ijk}$ | : control volume |
| $p$ | : pressure |
| $t$ | : time |
| $u$, $v$, $w$ | : stream-wise, span-wise, wall-normal velocity components |
| $z_0$ | : surface roughness |
| $D$ | : boundary layer depth |
| $C$ | : concentration of passive pollutant |
| $H$ | : height of hill |

| | |
|---|---|
| $K$, $\tilde{K}$, $K^{(\varepsilon)}$, $K^{(k)}$ | : turbulent diffusion coefficients |
| $\mathbf{L}$, $\mathbf{B}$, $\mathbf{D}$ | : space difference operators |
| $\vec{\Delta S}^{(l)}$ | : normal vector to $l$-th face of control volume |
| $\vec{F}$, $\vec{G}$, $\vec{H}$ | : inviscid fluxes |
| $\vec{R}$, $\vec{S}$, $\vec{T}$ | : viscous fluxes |
| $\vec{V}$, $\vec{W}$ | : velocity vector, vector of unknown variables |
| RANS equations | : Reynolds-averaged Navier-Stokes equations |

## References


[1] Castro I.P., Apsley P.P.: Flow and dispersion over topography: A comparison between numerical and laboratory data for two-dimensional flows, Atmospheric Environment, Vol. 31, No. 6, p. 839–850, 1996

[2] Bednář J., Zikmunda O.: Physics of atmospheric boundary layer, Academia, Prague, 1985 (in Czech)

[3] Jaňour Z.: On the mathematical modelling of stratified atmosphere, Institute of Thermodynamics, Report T-470/06, Prague, 2006 (in Czech)

[4] Sládek I., Kozel K., Jaňour Z., Gulíková E.: On the Mathematical and Numerical Investigation of the Atmospheric Boundary Layer Flow with Pollution Dispersion, In: COST Action C14 'Impact of Wind and Storm on City Life and Built Environment', von Kármán Institute for Fluid Dynamics, p. 233–242, ISBN 2-930389-11-7, 2004

[5] Beneš L., Sládek I., Jaňour Z.: On the Numerical Modelling of 3D-Atmospheric Boundary Layer Flow, In: 'Harmonization within Atmospheric Dispersion Modelling for Regulatory Purposes', Garmisch-Partenkirchen, Germany, p. 340–344, Vol. 1, ISBN 3-923704-44-5, 2004

[6] Bodnár T., Kozel K., Sládek I., Fraunié Ph.: Numerical Simulation of Complex Atmospheric Boundary Layer Flows Problems, In: ERCOFTAC bulletin No. 60: Geophysical and Environmental Turbulence Modeling, p. 5–12, 2004

[7] Sládek I., Kozel K., Jaňour Z.: On the 2D-validation study of turbulence $k$-$\varepsilon$ model including pollution dispersion, In: 'Topical Problems of Fluid Mechanics 2008', Institute of Thermodynamics, ISBN 978-80-87012-09-3, p. 101–104, Prague, 2008

[8] Wilcox D.C.: Turbulence modeling for CFD, DCW Industries, Inc., 1993

[9] Khurshudyan L.H., Snyder W.H., Nekrasov I.V.: Flow and dispersion of pollutants over two-dimensional hills, U.S. EPA, Report No. EPA-600/4-81-067, 1981

[10] Trombetti F., Martano P., Tampiery F.: Data sets for studies of flow and dispersion in complex terrain: 1) the RUSHIL wind tunnel experiment, CNR Technical Report No. 1, FISBAT-RT-91/1, 1991

[11] Almeida G.P., Durao D.F.G., Heitor M.V.: Wake Flows Behind Two Dimensional Model Hills, Exp. Thermal and Fluid Science, 7, p. 87, 1992

[12] Davroux A., Hoa C., Laurence D.: Flow Over a 2D Hill – Reference Solutions for $k$-$\varepsilon$ and Second Moment Closure Turbulence Models, Workshop, Karlsruhe, 1995

[13] Sládek I., Bodnár T., Kozel K.: On a numerical study of atmospheric 2D- and 3D-flows over a complex topography with forest including pollution dispersion, Journal of Wind Engineering and Industrial Aerodynamics, Vol. 95, Issues 9–11, p. 1422–1444, 2007

[14] Sládek I.: Mathematical modelling and numerical solution of some 2D- and 3D-cases of atmospheric boundary layer flow, PhD thesis, Czech Technical University, Prague, 2005

[15] Classic ERCOFTAC database at University of Surrey (online), http://www.ercoftac.org/


*Received in editor's office*: June 2, 2008
*Approved for publishing*: August 3, 2009

*Note:* This paper is an extended version of the contribution presented at the conference *Topical Problems of Fluid Mechanics 2008* in Prague.